Edge melting in low-coverage adsorbed films

D B Pengra† and J G Dash

Department of Physics FM-15, University of Washington, Seattle, WA 98195, USA

Abstract. A calorimetric study of low-coverage (0.13–0.36 layer) Ne films adsorbed on graphite foam explores the broadening of melting peaks in the vicinity of the two-dimensional triple point. Preliminary analysis confirms earlier indications that premelting is due to edge melting of long strips of film that decorate linear defects and steps on the substrate. A new model that incorporates these substrate effects and a new method of analysis that considers coverage-dependent trends have been developed to fit the data. The fitting indicates that additional substrate effects complicate the analysis; these are discussed, and it is concluded that adsorbate size effects are relatively unimportant, but that heterogeneity in the substrate binding energy may augment the edge melting process.

1. Introduction

1.1. Edge melting and its detection by calorimetry

Edge melting is the two-dimensional (2D) analogue of surface melting—it is the formation of a stable liquid or liquid-like layer of a substance at the interface between its solid and vapour at temperatures below the melting point. Surface melting has been observed in many materials with a variety of techniques [1,2,3], but experimental evidence for edge melting is comparatively rare—it has been indicated in heat capacity of neon on graphite [4], Mössbauer spectroscopy measurements of $Fe(CO)_5$ [5] and $Sn(CH_3)_4$ [6] on graphite, and most recently in STM images of the first layer of germanium (111) [7].

The phenomena of edge and surface melting are predicted as consequences of wetting [8]: if the liquid phase wets the interface between the solid and the vapour, then the system's free energy will be lowered by melting at the interface. Below the bulk melting point the formation of liquid is inhibited by the free energy cost of the heat of melting; thus there is a competition between the wetting energy and melting energy. The system's equilibrium establishes the molten layer's thickness that minimizes the superficial free energy. As the temperature of the system is raised toward the melting point, the cost of melting decreases and the liquid thickness diverges. At the melting point, a macroscopic thickness of liquid is present on the solid, and the interface is said to be *wetted* by the liquid.

Edge or surface melting may be derived from Landau–Ginzburg [9] or density-functional [10] theories, but the essentials may be illustrated by a simple mean-field theory. Such a theory, when developed for a semi-infinite system of van der Waals

---

† Present address: Risø National Laboratory, DK-4000 Roskilde, Denmark.

particles bound by a planar (in 3D) or linear (in 2D) interface, gives the result that the thickness of the liquid layer L_ℓ diverges as $|t|^{-1/p}$, where $t \equiv (T - T_t)/T_t$ is the reduced temperature with T_t being the temperature of the 'bulk' melting transition, and p depends on the dimensionality of the system. For unretarded forces, $p = 3$ for surface melting, and $p = 4$ for edge melting [4].

In a semi-infinite 2D system, however, large-scale fluctuations are expected to be present, rendering the mean-field predictions invalid; the upper critical dimension d^* of a 2D system is 11/5, thus $d^* > d$, where d is the physical dimension [11]. In such a fluctuation-dominated regime, the 2D disordered layer thickness should diverge as $|t|^{-1/3}$ instead of the mean-field prediction of $|t|^{-1/4}$ [12]. But fluctuations may be suppressed in the experimental system due to finite-size effects [4]. If the interface is of finite length Λ, the interface cannot support fluctuation modes with wavelengths longer than 2Λ. Additionally, we may imagine that if the system is not semi-infinite, but bound from below by a rigid substrate, height fluctuations will be constrained by the substrate [12].

In heat capacity experiments, edge or surface melting is indicated by a characteristic broadening of the melting peak toward lower temperatures. The peak is due to the conversion of solid to liquid at the transition. If the system undergoes ideal first-order melting at a triple point, the heat capacity of melting C_m would give a δ-function singularity at T_t, as $C_m = q_m \, dN_\ell/dT$, where q_m is the latent heat of melting, and in the ideal limit, N_ℓ, the number of particles in the liquid phase, would be a step-function centered at T_t. In the case of surface or edge melting, $N_\ell \propto L_\ell$, and the δ-function peak is broadened to a power law in the semi-infinite system: $C_m \propto dL_\ell/dt \propto |t|^{-(1+1/p)}$.

In thin multilayer films or low-coverage submonolayers, the proximity of the substrate will modify the surface or edge melting signal in a number of ways. First, if the substrate is only weakly attracting, the mere presence of the boundary will truncate the melting signal at a temperature below T_t, as the film will melt entirely by the premelting process. Second, the material closest to the substrate will not become completely disordered, as the solid boundary will tend to order those atoms into layers or rows. Thus, the specific entropy of melting will be less in thinner films or strips; this has been seen in neon and argon multilayers [13]. Third, as the film begins to surface or edge melt, the liquid/solid boundary, typically a few atoms wide, must form [14]. At the onset of melting, the dominant interactions are short-range repulsions; as such, the growth of the disordered layer is logarithmic with respect to $T - T_t$, and so there is predicted to be a crossover between -1 and $-(1 + 1/p)$ in the heat capacity signal's exponent [15]. This crossover behaviour has been seen in neon multilayers [13], where the heat capacity exponent tended from -1 toward $-4/3$ as the coverage became greater.

If the substrate attraction is greater, it may induce the more dense solid to wet the substrate/liquid interface above the melting point; this *substrate freezing* [16] is the complement of surface melting, as it is due to the same type of competition between wetting forces and the bulk heats of melting. Further, because of the competition between surface melting and substrate freezing, the power-law divergence in the heat capacity is rounded to a peak. In the absence of significant strain effects, the substrate attraction will always cause the melting heat capacity signal approaching the peak to follow a curve that is weaker than the power law predicted by the asymptotic theory, but the location of the peak itself may be higher or lower than T_t, depending upon the substrate attraction, as will be demonstrated below.

A still stronger attraction may complicate the melting signal further. Compression of the adsorbate has been invoked to explain incomplete wetting [17, 18]. Such an effect may be incorporated into surface melting theory as a perturbation on the solid density, with the result that strained thin films will more readily surface melt, as the strains sustained by the adsorbed solid are released upon melting [19]. The combination of surface melting, substrate freezing and strain release will cause the melting peak of a thin, strained film to shift to lower temperatures and become sharper in proportion to the amount of strain in the solid. This theoretical distinction between strained and unstrained films is seen experimentally in a comparison of the melting peaks of Kr films with Ar or Ne films [19].

1.2. Crystal defects and the decoration of graphite

Many investigations [5, 6, 20, 21, 22, 23] of submonolayer films adsorbed on graphite have assumed that the adsorbed crystallites form patches or free-standing islands, but the actual shape of the crystallites has not been determined. We argue here that a careful consideration of the graphite surface and the present knowledge of the physics of surface decoration indicates that the most likely crystallite morphology is long strips, coextensive with and bound to linear defects in the surface.

Decoration of crystal defects by adsorbates is a commonly observed phenomenon, indeed it has been used as a tool to examine more closely the nature of defects and growth steps in crystals. Pioneering work by Bethge [24] and collaborators showed that monatomic growth steps in alkali halides could be revealed by vapour deposition of gold followed by annealing. The gold atoms clump together and migrate to the steps, forming clusters along the step boundary; these clusters are visible by now standard techniques in electron microscopy. The same phenomenon has been observed in gold adsorbed on graphite [25]. It appears that the coalescence of the gold clusters can occur through at least three different mechanisms: Ostwald ripening, or diffusion of single atoms away from smaller crystallites to larger crystallites; crystallite motion, where whole crystallites in motion bump into each other and stick; and coalescence during growth [26]. In these ways, the decoration of the growth steps mimics the growth of the substrate crystal itself: atoms impinging on the surface stick, and if the temperature is high enough, migrate to sites of stronger binding and cohere with other adsorbate atoms.

We expect low coverages of neon adsorbed onto the surface of graphite to behave in a similar manner, with an important exception: the adsorbate remains a film which does not coalesce into three-dimensional clusters. Evidence for this claim is strong, as it is clear from thermodynamic studies [20, 27] that the phase transitions of the neon/graphite monolayer system occur at significantly lower temperatures than those for bulk neon [28]. Further, it appears that annealing the films significantly sharpens the transitions and improves the reproducibility of the results [27]; this indicates that the atoms indeed move about the surface of the graphite and coalesce into larger and more stable structures. The most probable morphology adopted by the neon adsorbate is a collection of crystallites of monatomic thickness coalesced at defects, steps, and other inhomogeneities present on the graphite surface.

Graphite foam, the substrate used in this experiment, is a form of exfoliated graphite made by lightly compressing tiny 'worms' of exfoliated crystals into a large piece that can be subsequently cut into experimentally useful shapes [29]. To the naked eye, foam appears to be highly heterogeneous, but x-ray lineshape analysis [30]

and analysis of vapour-pressure measurements [31] indicate that crystal coherence lengths are on the order of 1000 Å.

The process that turns natural graphite crystals into foam introduces copious defects into the crystal lattice. Because of the layered structure of graphite, in which carbon atoms are bound covalently in hexagonal nets that are in turn stacked via van der Waals forces to form a three-dimensional structure with a hexagonal unit cell, the layers of the graphite can move easily against one another [32]. It is not surprising, then, that the predominant type of dislocations in graphite are in the basal plane [33]. These give rise to stacking faults [34], twins [35], and more general deformations of the basal planes [36]. In a given crystal of graphite, many defects lie buried within and form complex arrays of dislocation ribbons and patterns of ribbons, as is seen with transmission electron microscopy [34]. Yet some of these dislocations can propagate through the crystal forming simple tilt boundaries evident at the surface.

Particularly low-energy types of tilt boundaries are created by twins, which preserve the hexagonal unit cell on either side of the boundary. Tilt boundaries due to twins are found to be the loci of fractures that develop when the crystal is stressed [37]. Consequently, the presence of twins is responsible for long striae [36] and straight steps on the surface of a graphite crystal, as well as the low strength of graphite in general [37].

Due to the linear nature of graphite crystal defects, it appears that the dominant morphology of the adsorbed neon crystallites should be long strips coextensive with linear steps. That this particular morphology should obtain in the monolayer system is especially interesting, for it extends the analogy between 3D bulk systems and 2D surface systems to include 1D line systems, as we may imagine the steps and tilt boundaries to form 'one-dimensional substrates' on which are adsorbed strips of condensed neon. This, then, comprises the operative physical picture of submonolayer coverages of graphite elaborated in this paper. By analogy with surface melting, the strips are imagined to begin their melting at the free edge; the boundary of the melt moves into the strip as the temperature is raised, and the melting ceases when the boundary reaches the 1D substrate—the graphite defect.

2. Experiment

The neon/graphite submonolayer system was selected for this edge melting study, because in many ways it appears to be a 2D analogue of 'classical' 3D van der Waals system [20,22,23,38]. In the temperature/coverage plane, it possesses a 2D triple line at 13.4 K extending from 0.1 to 0.6 monolayer, and a 2D critical point at 15.6 K and 0.4 monolayer [27]. Thermodynamic analysis of calorimetry data taken on a less homogeneous substrate, Grafoil [29], has produced estimates of the latent heats of sublimation, vapourization, and (consequently) melting at the triple point to be 86 K, 24 K, and 62 K, respectively [39].

Our apparatus, an adiabatic calorimeter, was the same as used for recent studies of surface melting in argon [3], neon [13], and krypton [19], and a previous study of edge melting in neon monolayers [4]. The sample cell is a copper container filled with uncompressed exfoliated graphite foam [29]. Monolayer coverages are calculated using 133.3 cm^3 STP equal to 1.0 monolayer.

Seven coverages were studied in enough detail to admit analysis. They range from 0.13 to 0.36 equivalent monolayers. In the region of the melting peak, typical
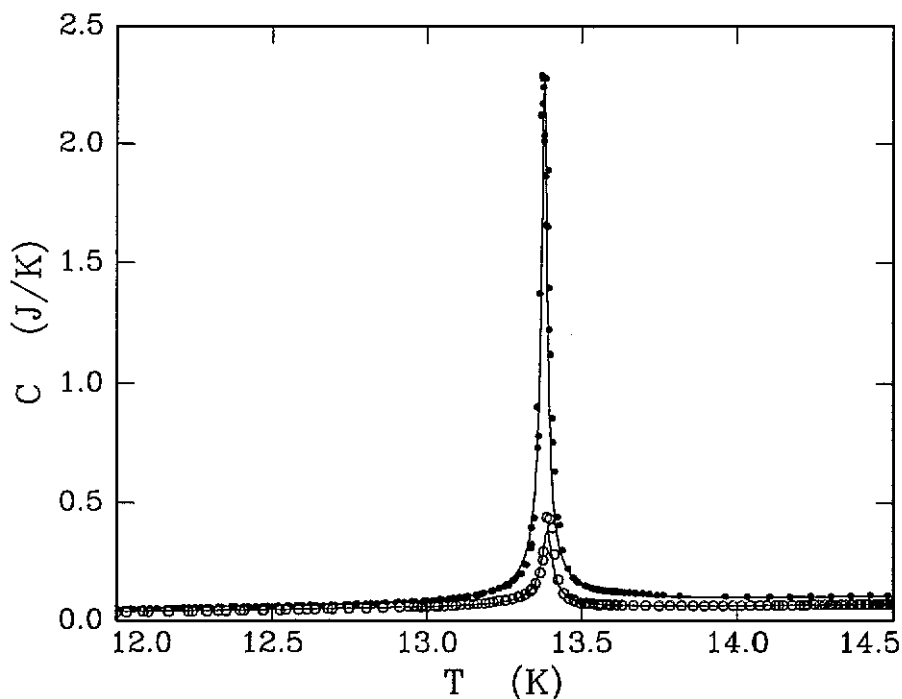
Figure 1. Heat capacity data of 0.13 layer (o) and 0.36 layer (•) coverages, superimposed. Solid lines are fits according to the model described in the text. The data for the other coverages studied falls in between these two (see figure 4).

point-to-point temperature steps are 0.01 K or less. The melting peak region was examined at least three times per sample in order to establish reproducibility.

Figure 1 shows the heat capacity of 0.13 monolayer and 0.36 monolayer super-imposed; the data for the other coverages falls in between these. The strong central peak at 13.4 K marks the triple point. The slow increase in the heat capacity with temperature below this point is due principally to sublimation, as will be argued in section 4.

A look at the region around the melting peak with an expanded temperature scale (figure 4) shows that the dependence of the melting peaks on coverage is not what was seen in an earlier study by Zhu, Pengra, and Dash (ZPD) [4], which was done with the same apparatus and adsorbate, but with higher coverages (0.42 and 0.57 monolayers). In ZPD, the low-temperature edges of the peaks were aligned, and the location in temperature of the highest point of each peak increased with increasing coverage (see figure 2 in ZPD). Here, however, the leading edges, or *precursors* are clearly separated, and the peak locations tend to remain stationary with increasing coverage. The different coverage-dependent behaviour indicated that the simple, asymptotic model of edge melting used by ZPD may be insufficient to account for the melting-peak broadening in the low-coverage neon system. We consider now the influence of a substrate field, which should be significant in the case of low coverages, on a model system.
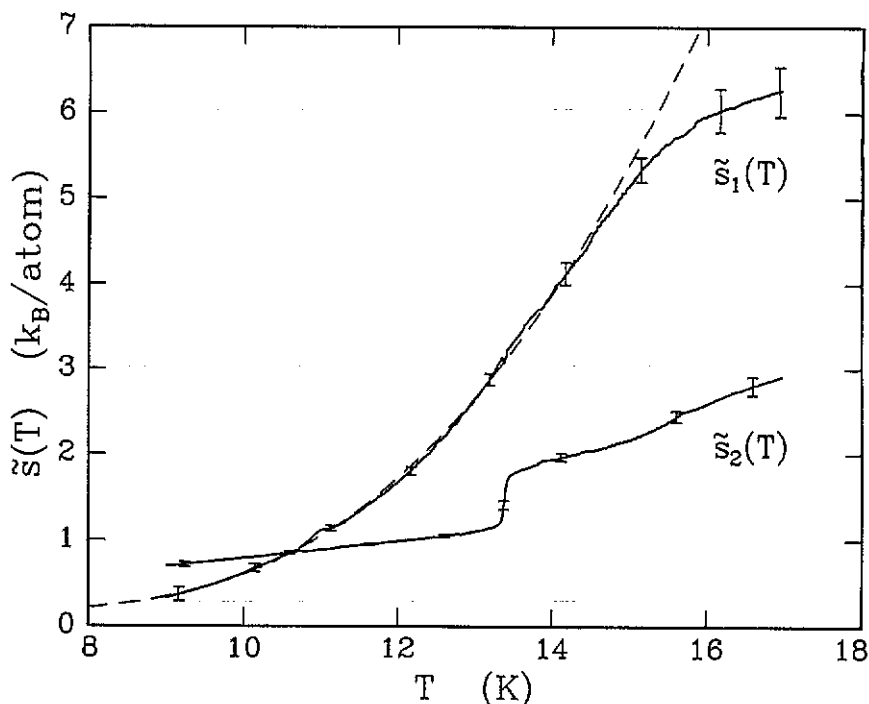
Figure 2. The empirical curves $\tilde{s}_1(T)$ and $\tilde{s}_2(T)$ plotted on a common scale. The dashed line through $\tilde{s}_1(T)$ is a fit to a simple 2D sublimation model as described in the text. The error bars, equal to one standard deviation, indicate the approximate scatter of the data about the curves.

3. Theory

In the context of multilayer film studies, some of the results of the calculation presented in this paper have been given before [19, 16, 40, 41]. Refer to [42] for the details of the approach we have followed here. The calculation is based on the sharp-kink approximation [43], which assumes that the film is made up of uniform phases separated by sharp, linear boundaries. We derive an equation of state for a strip of adsorbate of moderate to large width (> 10 atomic layers). The balance of interfacial energies stratifies the strip into two regions, a 2D solid of density ρ_s and width L_s bound on one side by an attractive substrate of density ρ_w and on the other side by a 2D liquid of width L_ℓ and density ρ_ℓ, which is in turn bound by a bulk 2D vapour of density ρ_v. The proportion of liquid to solid is controlled by proximity of the bulk phase transition, which is given by the difference of the bulk chemical potentials of the liquid and solid phases, $\mu_\ell - \mu_s$:

$$c(\mu_\ell - \mu_s) = (\sigma/L_\ell)^4 + (1 - \zeta)(\sigma/L_s)^4 . \tag{1}$$

In deriving (1), the interaction potentials are assumed to have a non-retarded van der Waals attractive tail (that varies as r^{-6}), and a repulsive hard core of diameter σ; integration of the potentials increases the exponent of -6 to -4. The coupling coefficient between adsorbate atoms is assumed to have strength α, and that between adsorbate and substrate atoms strength β. The parameter $\zeta = \rho_w \beta (\rho_s \alpha)^{-1}$ controls

the degree to which the behaviour of the strip differs from that of the semi-infinite system. If $\zeta = 1$, we recover the asymptotic result used in ZPD. The quantity c we take as a lumped constant equal to $32\rho_\ell\sigma^4[3\pi\alpha(\rho_s - \rho_\ell)(\rho_\ell - \rho_v)]^{-1}$.

For further analysis, we make the following approximations. First, to obtain the temperature dependence, we expand $\mu_\ell - \mu_s$ to first order in temperature about the triple point; hence, $\mu_\ell - \mu_s = -q_m t$, where q_m and t are the latent heat of fusion and the reduced temperature, as defined in the introduction. Further, we assume that in the temperature range of melting, most of the particles of the solid are converted to liquid, and very few are promoted into the vapour; that is, we assume an approximate particle conservation of the form $\rho_s L_s^0 = \rho_s L_s + \rho_\ell L_\ell$, where L_s^0 is a constant equal to the width of the strip well below T_t. Now, by defining the dimensionless lengths $l \equiv L_\ell/\sigma$ and $n \equiv L_s^0/\sigma$ and a parameter $\delta \equiv \rho_\ell/\rho_s$, and then making the change of variables $l' \equiv \delta l/n$, $\epsilon \equiv [\zeta - 1]/\delta^4$ and $c' \equiv cq_m/\delta^4$, we may rewrite (1) in terms of dimensionless quantities:

$$c'n^4 t = l'^{-4} - \epsilon(1 - l')^{-4} . \tag{2}$$

Physically relevant values of l' are bound by 0 and 1 for any n.

In general, the peak of the heat capacity of melting does not occur at $t = 0$. The heat capacity due to melting is highest where the rate of conversion from solid to liquid is greatest. Thus, the location of the melting peak is also the location of the extremum of dl'/dt. A simple calculation shows that the position of the peak is given by

$$t_p = (1 + \epsilon^{1/6})(1 - \epsilon^{1/3})/n^4 c' . \tag{3}$$

This result is experimentally significant. First, as the total coverage N increases, which implies that n increases, the melting peak position T_p tends toward the triple-point temperature T_t according to $T_p - T_t \propto n^{-4}$. Second, the sign of the trend, that is, whether the peaks move downward or upward in temperature with increasing n, depends on the value of ϵ. If $\epsilon > 1$, then the peaks will move downward toward T_t with increasing n, as $c' < 0$. On the other hand, if $\epsilon < 1$, then the peaks will move upward with increasing coverage toward T_t. This behaviour has been seen in case of Ar multilayers [3], where the melting-peak temperature of successively higher coverages was found to approach T_t from below according to $T_t - T_p \propto (N - N')^{-3}$, with N' a constant. In the Ar study, this temperature trend was attributed to a simple truncation of surface melting as the boundary of the melt reached the substrate, a scenario equivalent to setting $\zeta = 1$ or $\epsilon = 0$ in an equivalent 3D theory. The argument here shows that the power-law dependence of the peak location is more general than what might be expected from the simple truncation scenario.

Only if $\epsilon = 1$ then does $t_p = 0$; at this value, the locations of the melting peaks remain stationary with respect to the coverage, and equal to T_t. Note that if the substrate attraction is sufficiently strong ($\zeta > 2$), then the melting peaks will always be at temperatures *higher* than T_t for any reasonable values of the liquid and solid densities.

We may derive relationships concerning the height and width of the specific heat peak as well. Since dl'/dt is proportional to the specific heat of melting c_m, we find

$$c_m(t = t_p) \propto -c'n^4/[4(1 + \epsilon^{1/6})^6] . \tag{4}$$

This shows that the height of the specific heat peak scales according to n^4, and, to leading order, is inversely proportional to ϵ. Further, we find that the width of the specific heat peak Δt_p has the functional form $\Delta t_p = f(\epsilon)(c'n^4)^{-1}$, where $f(\epsilon)$ depends only on ϵ.

Solution of the model equation (2) involves finding the relevant root of an eighth-order polynomial, which may be easily performed by standard techniques in computational analysis. A broader question involves the incorporation of (2) into the analysis of the calorimetric data, to which we will now turn our attention.

4. Analysis of the data

In contrast to the earlier multilayer studies done in our laboratory [3, 13, 19], the calorimetric detection of edge melting is hampered by two difficulties unique to sub-monolayer systems. First, the 'true' value of T_t is poorly known and not easily measurable *in situ*. In multilayer measurements, T_t is equal to the 3D bulk value, and it may be measured by dosing the cell with a large quantity of adsorbate. Second, the heat capacity of melting is comparatively weak; sublimation and evapouration processes and the intrinsic specific heats of the adsorbed phases contribute a significantly greater portion than in the multilayer measurements; the separation of the melting signal from these other contributions we shall call the 'background' problem.

In an attempt to solve these problems by treating all of the data for the various coverages in a systematic way, and thereby uncover trends in T_t and the background, we have discovered that the entropy of the films—the integrated heat capacity—can be separated into two parts. Specifically, the entropy of each sample between 9–17 K is well represented by

$$S(N, T) = N_1 \tilde{s}_1(T) + (N - N_1)\tilde{s}_2(T) \tag{5}$$

where N_1 is an arbitrary constant, and $\tilde{s}_1(T)$ and $\tilde{s}_2(T)$ are empirically determined functions of the temperature that depend on N_1; these are shown in figure 2. That N_1 may be arbitrarily chosen is a strong indication that the adsorbed film is composed of two coexisting phases over much of the temperature range studied. This finding is supported by previous investigators of this system [20, 27] who used a result by Stewart and Dash [44] that the entropy and heat capacity of a two-phase film should be a linear function of the coverage N; that is, $S(N, T) = N f(T) + g(T)$. Clearly (5) has this form for any nonzero N_1.

The particular value of N_1 chosen here is made to force the melting transition—a 'step' in the entropy curves—to be seen in only $\tilde{s}_2(T)$. It may be shown [42] that if the amount of matter in the 2D vapour phase N_v depends only weakly on the total dosage N (but may depend strongly on T), the choice of N_1 that 'nulls' the step in $\tilde{s}_1(T)$ is equal to N_v at T_t. The assumption that N_v is largely independent of N is not independently supported by the data, but a check on the self-consistency of the argument indicates that N_v would vary about 7% over the range of coverages studied given the determined value $N_1 = 0.07$ monolayer [42].

We now consider whether the separation of the entropy into contributions from the various phases can be extended to temperatures below T_t. Regarding the vapour phase, we expect that the temperature dependence of its entropy will be due to the intrinsic entropy of the phase, and the promotion of atoms into the phase from the

solid. An elementary calculation of 2D solid sublimation to a 2D ideal gas gives, to leading order in T, a model entropy

$$S_v^{(\text{mod})}(T) = \left(\frac{\alpha q_s}{k_B T}\right) e^{-q_s/k_B T} \tag{6}$$

where α is a constant, and q_s is the latent heat of sublimation. A fit of (6) to $N_1 \tilde{s}_1(T)$ from 9–14 K (shown by the dashed line in figure 2) gives $q_s/k_B = 89.2$ K, which is in good agreement with a previous study [39]. This suggests we may regard $N_1 \tilde{s}_1(T)$ as largely representing the entropy of the vapour plus sublimation, and $(N - N_1)\tilde{s}_2(T)$ as the entropy of a 2D condensate that melts at about 13.4 K.

In the sharp-kink approximation, the entropy depends only on the entropies of the bulk phases; no extra contribution comes in from the interfacial terms [42]:

$$S(N, T, A) = N_v s_v(T) + N_\ell s_\ell(T) + N_s s_s(T). \tag{7}$$

This result is a consequence of the assumptions of the absence of excess matter at the interfaces, the uniformity of the bulk material, and the fact that the interfacial energies depend only implicitly on the temperature. We let $\Delta s_{\ell s}(T) \equiv s_\ell(T) - s_s(T)$ and $N_v = N_1 + \delta N_v(T)$ and rearrange the above as

$$S(N, T, A) = N_1 \left(\frac{N_v s_v(T)}{N_1}\right) + (N - N_1)\left(s_s(T) + \frac{N_\ell}{N - N_1}\Delta s_{\ell s}(T)\right)$$
$$+ \delta S(T) \tag{8}$$

where $\delta S(T)$ is a correction that incorporates the decrease in the entropy of the condensed phase by promotion into the vapour, and the change in the entropy of the liquid phase through the dependence of the amount of liquid on the total width of the adsorbed strip. An approximation used in the above modelling of $S_v(T)$—that the change in entropy due to promotion is principally due to the increase of the population of the vapour, and the approximation used in section 3 to solve the equation of state—that, in the temperature range of the melting transition, the thickness of the liquid strip is only weakly altered by evapouration—are sufficient to render $\delta S(T) \approx 0$.

Consequently, within these approximations, we find that $\tilde{s}_2(T) = s_s(T) + l' \Delta s_{\ell s}(T)$, where $l' \equiv L_\ell \rho_\ell (L_s^0 \rho_s)^{-1} = N_\ell[N - N_1]^{-1}$, and $\tilde{s}_1(T) = (N_v/N_1)s_v(T)$. Now, we incorporate the results of the edge melting model: l' is given by the solution of (2).

Specifically, we create a model entropy $S^{(\text{mod})}(N, T)$ from (8) by approximating the specific entropies of the liquid and solid, $s_\ell(T)$ and $s_s(T)$, by linear functions of the temperature, and then fit the result

$$S^{(\text{mod})}(N, T) = S_v^{(\text{mod})}(T) + (N - N_1)\left[s_s^{(\text{mod})}(T) + l' \Delta s_{\ell s}^{(\text{mod})}(T)\right] \tag{9}$$

by adjusting T_t and n (which control l') by hand, and allow the coefficients in $s_s^{(\text{mod})}(T)$ and $\Delta s_{\ell s}^{(\text{mod})}(T)$ to be found by the method of linear least squares. The results are shown in figure 3.

The method gives good representations of the heat capacity over a wide range of temperature (11–15 K) by simple differentiation of (9):

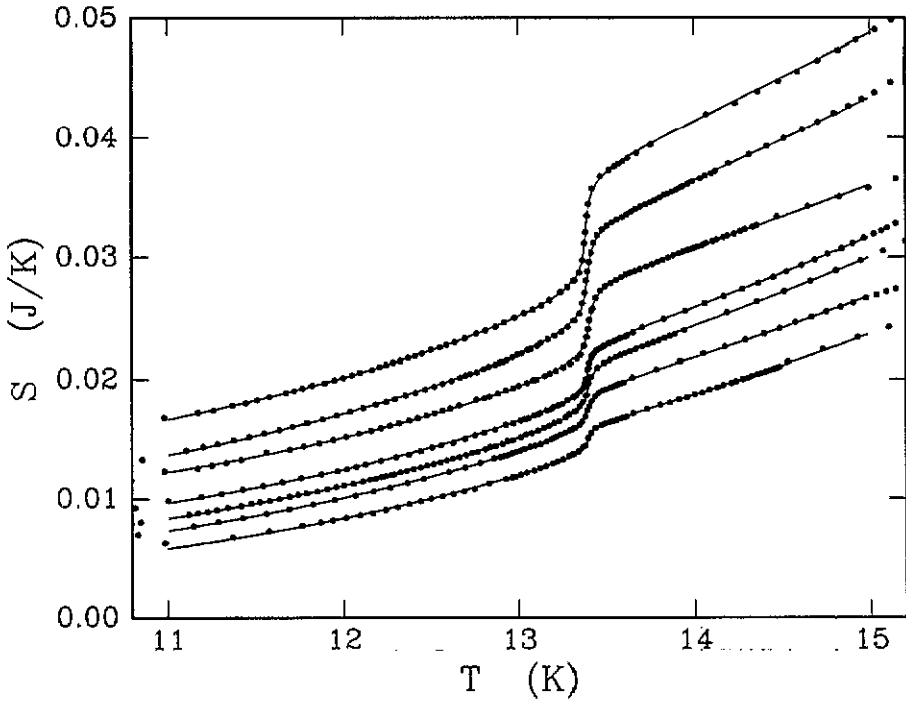$$C^{(\text{mod})}(T) = T(\mathrm{d}S^{(\text{mod})}(T)/\mathrm{d}T). \tag{10}$$

Figure 3. The entropy of the neon films (vertical ordering corresponds to order in coverage, from lowest to highest). The solid lines represent the best fit of the model for each sample. (For clarity, only every other data point in each set is shown.)

The entropy fits are shown in figure 3 and the resulting heat capacity curves are shown in figures 1 and 4 by the solid lines through the data points. No improvement was found by directly fitting the heat capacity; indeed such effort gave generally poorer results, probably due to the sensitivity of the fitting algorithm to scatter of the data in the peak.

By this analysis, the background problem is handled in a new way from that in ZPD; there, the background was chosen arbitrarily: a line was fitted to the heat capacity data from 10–12 K and extended underneath the melting transition. Then, the power-law fit was optimized by varying T_t and fitting the difference between the line and the data in the peak. Yet, upon further consideration, we have found that the exponent derived from this manner of fitting is unreliable; different arbitrary backgrounds give different best-fit exponents. In effect, the method in the present study differs from the previous one in that the value of the 'exponent' (the true power law obtains only in the semi-infinite limit) is fixed to the mean-field prediction, and then the background is automatically optimized for different values of T_t and strip thickness n.

The individual fits to the data represent the data extremely well. Yet, given the number of free parameters (six) and the simplicity of the entropy curves, we do not regard this result in itself as a vindication of the edge-melting model. The test of the model lies in whether the coverage-dependent trends of T_t and n conform to the assumptions which generated it.

The theory requires T_t to be constant; we find that $T_t = 13.39 \pm 0.01$ K, which is
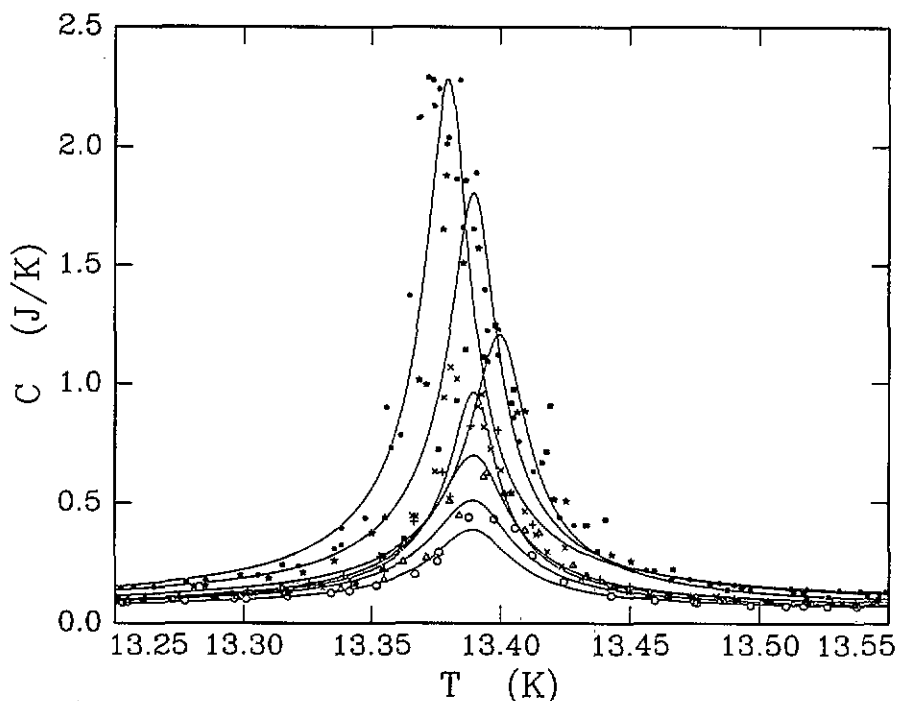
Figure 4. Collected heat capacity data in the region of the strongest peak. The solid lines are best fits according to the analysis of section 4. The peaks are ordered from weakest to strongest in terms of cell dosage; shown here are 0.13 (O), 0.15 (△), 0.18 (+), 0.21 (×), 0.26 (■), 0.31 (⋆), and 0.36 (•) monolayers.

constant to within our resolution, so this first expectation is satisfied. A test of the peak shift predicted by (3), however, is not possible; estimates of the parameters c' and ϵ that enter into (3) indicate that the peak should show a very slight shift downward in temperature with increasing coverage, yet this trend is well within the scatter in the peak locations.

The film-growth scenario described previously assumes that the adsorbate builds solid strips along linear defects in the graphite. Hence, we expect that n should be proportional to the part of the dosage that forms strips on clean crystal, as the other part goes into 2D vapour, 3D vapour, and matter bound tightly at a heterogeneous collection of sites (which may not participate in the thermodynamics at the experimental temperatures). If we take N_{excess} to be the number of atoms that make up this second part of the coverage, and $A_{\text{heterogeneous}}$ to be the area of the tight-binding sites, then $n \propto (N - N_{\text{excess}})/(A - A_{\text{heterogeneous}})$. Consequently, n should be a linear function of the coverage which goes to zero somewhat before zero coverage.

We may estimate expected values of n by the following simple argument. If we imagine all of the strips in the experimental cell as parts of a single long strip of maximum width W (that is $A - A_{\text{heterogeneous}} = W\Lambda$) then the substrate should be decorated with strips of width

$$n = [(N - N_{\text{excess}})/N_0] W/\sigma. \tag{11}$$

If we take $N_{\text{excess}} = 0.07 N_0$, as deduced by the entropy analysis, $\sigma = 3.16$ Å [45],

and $W = 1000$ Å, then for the range of coverages studied, n should be 25–91σ.

The fitting procedure produces values of n that vary approximately linearly from 7.4 for 0.13 monolayer coverage to 8.6 for 0.36 monolayer coverage. These values are not only substantially below what is expected, but the trend would indicate a film of strips of width 6.8 σ at zero coverage, which clearly violates the assumptions of the model. Further, we note that an error in the parameters c' or ϵ would only alter the values of n by a simple multiplicative constant and not change the general dependence of n on the coverage.

5. Discussion: alternative explanations of peak broadening

The discrepancies in the trend of n versus coverage force the conclusion that the simple edge melting model is not adequate to explain the detailed behaviour of the melting of neon films. We now turn to a consideration of other possible features that might be required in a model description.

First, we expect the sharp-kink approximation to fail at the beginning and end of the melting of an otherwise uniform adsorbate patch; in these limits, the width of the 'phase' is comparable to the width of the interfaces that border it. The entropy associated with the formation of the liquid/solid interfacial region is less than that associated with complete melting, as the region itself has characteristics intermediate between the solid and the liquid; the heat capacity and total melting entropy are thereby reduced from those expected from the sharp-kink model. Furthermore, the temperature dependence at the beginning of melting would be altered from the predicted power law; the formation of the interface involves the short-range interactions of the atoms, and consequently, the heat capacity would begin to grow logarithmically until the interface is fully formed [15, 13]. These effects would produce logarithmic 'wings' on the melting peaks which would be of constant strength with respect to the coverage. As the coverage increased, a sharper peak that conformed to our theory would rise out of the centre of the broader peak. The widths of the interfaces, then, should only be seen as an effective reduction of n by a constant, once the coverage has become sufficiently large.

Alternate explanations of melting-peak broadening that do not consider edge melting have been proposed. For monolayer systems, these have considered the role of substrate imperfections which give rise to two related effects—finite crystallite sizes and binding-energy heterogeneity [46].

In the first case, the polycrystalline surface of the substrate does not allow a large, unbroken adsorbate phase to form; contiguous regions are limited by the sizes of 'good crystal' present in the cell. The adsorbate is thus broken up into a collection of small, independent patches. Finite-size effects have been claimed to explain melting-peak broadening in O_2 monolayers adsorbed on Grafoil [21]. The theory of finite-size effects in first-order phase transitions has become quite complex and will not be addressed here (see [47, 48, 49]); rather, we appeal to a simple argument given by Imry [48] in order to estimate the importance of finite-size effects for the Ne/graphite foam system. Arguing from simple results in the theory of fluctuations, Imry proposed that a first-order transition should be broadened according to

$$\Delta T_c / T_c \sim 1 / (N_{\text{patch}} \, \Delta s) \tag{12}$$

where N_{patch} is the number of particles in a contiguous patch and Δs is the latent entropy of transition measured in units of k_{B}, and T_{c} is the transition temperature, here equal to T_{t}. If we take $\Delta T_{\text{t}} = 0.05$ K as an estimate of the width of a typical melting peak, and $\Delta s = q_{\text{m}}/T_{\text{t}}$ from the preceeding section, then according to (12), $N_{\text{patch}} \approx 230$, which would indicate average patch sizes of about 15 atoms across. Using data from Marx [21] data for O_2 adsorbed on Grafoil in (12) gives a patch size of about eight molecules across, which is about a factor of three smaller than Marx found by using a more sophisticated theory and fitting procedure.

Neutron diffraction work with neon adsorbed on Grafoil indicates that the typical neon coherence lengths are 160 Å, or about 50 atoms across [23]; this is about the same size as measured for the Grafoil crystallites themselves, but the graphite crystallites in foam are much larger—about 1000 Å across [30]. If typical neon patch sizes on foam are actually 45 atoms across, as estimated from peak broadening by Imry's result times 3, or about the same size as those seen in Grafoil with neutrons, then the neon crystallite domains would be approximately the size of a typical Grafoil domain but only 2–3% of a typical graphite foam domain.

There are, however, at least two other possible mechanisms by which small crystallites may obtain in this system. First, we may have a 2D analogue of incomplete wetting (see [8]), whereby the strips are limited in width to a few σ and the excess material forms free-standing islands. Such a situation may be expected if the step attraction is either too weak (in which case the adsorbate easily breaks away to form free-floating islands) or too strong (in which case the strain energy sustained by the adsorbate is greater than the energy of wetting).

Second, at many places in the adsorbing surface, strip growth may be suppressed at those defects that do not form an attractive step, such as unbroken twin boundaries, because the crystallites may prefer a particular orientation with respect to the substrate lattice that is not maintained across the defect [50]. In this case, there may be an effective repulsion at the defect, instead of an attraction, due to the variation in epitaxial energy.

The second effect of substrate imperfections, often simply called *energy heterogeneity* [46,50], is due to variations in the binding energy attributable to inhomogeneities in the local structure of the substrate. Energy heterogeneity affects phase transitions of an adsorbate principally by causing variations in the adsorbate's local density; hence, the melting temperature varies over the film according to local phase boundaries.

Indeed, heterogeneity effects have been invoked to model the high-temperature side of the melting transition in an earlier study of neon edge melting [4]. In this scenario, the adsorbed material is compressed and its melting point is raised proportionally to the local strength of the substrate field; thus the shape of the higher-temperature side of the melting peak mirrors the binding-energy density of states; when the temperature T is increased, the amount of material brought into the transition is proportional to the amount of material bound by the substrate at an energy $k_{\text{B}}T$. With increasing coverage, the envelope of the melting peak shifts upward in temperature because melting begins at the same point independent of coverage—the onset of melting being defined by the conditions at the solid/vapour interface. In the earlier treatment, edge melting and energy-heterogeneity broadening were treated as independent phenomena, which is valid if binding-energy variations are small at the free edges of the adsorbed strips.

In some respects, energy heterogeneity and finite-size effects are assumed by the stratified-strip model: there must be sites of preferential adsorption in the cell in

order to form the strips, and there must be a lot of them in order to have sufficient edge length so that the premelting signal will be strong enough to measure. But the essential physics of the model assumes an otherwise perfect substrate. We remark that including heterogeneity effects fully into the theory which produced (1) would make it considerably more complicated, and also less useful, as it would increase the number of adjustable parameters by the inclusion of the 2D compressibilities of the solid and the liquid.

6. Conclusions

The analysis given above was conceived when it became apparent that the older approach used in ZPD was not sufficient to explain the new data, nor was it sufficiently robust to validate the simple asymptotic model of edge melting. The present approach, which treats the whole system, including the coverage N, and thereby examines a larger portion of the thermodynamic space occupied by it, shifts the test of the theory from whether the desired exponent can be found to whether the width parameter n, which can be independently estimated from known experimental parameters, behaves as expected. Further, the new approach treats the background problem systematically, and provides high-quality fits to the data over a much greater temperature range than in ZPD. In these ways the test of the model is made more robust.

Alas, the simple model has been found to be lacking. Consideration of possible complicating effects, outlined above, suggests that substrate heterogeneity influences the melting transition significantly. It is the only mechanism whose influence would remain large as the coverage increased; present knowledge of the likely adsorbate morphology favours strip formation; in this case, finite crystallite sizes and interfacial widths should become less important at higher coverages. Yet, energy heterogeneity alone is not sufficient to explain the melting peak behaviour, as it cannot account for the melting-peak width below T_t [4]. Thus, we believe that the broadening is due to edge melting augmented by heterogeneity effects.

The preceding analysis has shown that heat capacity measurements alone are not sufficient to prove that edge melting, in whatever form it might take, occurs in this system; the data are too simple to allow one to determine among complex scenarios of melting. Yet, we have been able to decide against a too simple scenario, and thus we can suggest new directions for research to proceed. Foremost would be a direct determination of the sizes and shapes of the adsorbed crystallites; such a measurement would resolve the question of finite-size effects unambiguously, and it would reveal whether a strip formation process does indeed occur. In theory, one could determine the decoration morphology by line-shape analysis of high-resolution x-ray diffraction data [52], but in practice such an approach may be hampered by the small scattering cross-section of the adsorbate. A more promising approach may be with new methods of microscopy, of which [7] is an example using STM.

References

[1] Dash J G 1989 *Contemp. Phys.* **30** 89
[2] van der Veen J F, Pluis B and Denier van der Gon A W 1988 *Chemistry and Physics of Solid Surfaces VII (Springer Series in Surface Science 10)* ed R Vanselow and R F Howe (Berlin: Springer)
[3] Zhu Da-Ming and Dash J G 1986 *Phys. Rev. Lett.* **57** 2959
[4] Zhu Da-Ming, Pengra D and Dash J G 1988 *Phys. Rev.* B **37** 5586
[5] Shechter H, Brener R and Suzanne J 1988 *Europhys. Lett.* **6** 163
[6] Shechter H, Brener R, Folman M and Suzanne J 1990 *Phys. Rev.* B **41** 2748
[7] Feenstra R M, Slavin A J, Held G A and Lutz M A 1991 *Phys. Rev. Lett.* **66** 3257
[8] Dietrich S 1988 *Phase Transitions and Critical Phenomena* vol 12, ed C Domb and J Lebowitz (London: Academic)
[9] Lipowsky R 1982 *Phys. Rev. Lett.* **49** 1575
[10] Ohnesorge R, Löwen H and Wagner H 1991 *Phys. Rev.* A **43** 2870
[11] Lipowsky R 1984 *Phys. Rev. Lett.* **52** 1429
[12] Schick M 1990 *Les Houches, Session XLVIII, 1988—Liquides aux interfaces/Liquids at interfaces* ed J Charvolin, J F Joanny, and J Zinn-Justin (Amsterdam: Elsevier)
[13] Zhu Da-Ming and Dash J G 1988 *Phys. Rev.* B **38** 11 673; *Phys. Rev. Lett.* **60** 432
[14] An Guozhong 1989 *PhD Thesis* University of Washington
[15] Löwen H, Beier T and Wagner H 1989 *Europhys. Lett.* **9** (8) 791
[16] Pettersen M S, Lysek M J and Goodstein D L 1989 *Phys. Rev.* B **40** 4938
[17] Huse D A 1984 *Phys. Rev.* B **29** 6985
[18] Gittes F G and Schick M 1984 *Phys. Rev.* B **30** 209
[19] Pengra D B, Zhu Da-Ming and Dash J G 1991 *Surf. Sci.* **245** 125
[20] Huff G B and Dash J G 1976 *J. Low Temp. Phys.* **24** 155
[21] Marx R 1989 *Phys. Rev.* B **40** 2585
[22] Tiby C, Wiechert H and Lauter H J 1984 *Surf. Sci.* **119** 21
[23] Wiechert H, Tiby C and Lauter H J 1981 *Physica* B **108** 785
[24] Bethge H 1981 *Interfacial Aspects of Phase Transformations, Proc. NATO Advanced Study Inst. 1981* ed B Mutaftschiev (Dordrecht: Reidel) pp 669–696
[25] Heyraud J C and Metois J J 1980 *J. Cryst. Growth* **50** 571
[26] Kern R 1982 *Interfacial Aspects of Phase Transformations, Proc. NATO Advanced Study Inst. 1981* ed B Mutaftschiev (Dordrecht: Reidel) pp 303–314
[27] Rapp R E, de Souza E P and Lerner E 1981 *Phys. Rev.* B **24** 2196
[28] Crawford R K 1977 *Rare Gas Solids* vol 2, ed M L Klein and J A Venables (New York: Academic)
[29] Grafoil and graphite foam are products of the Union Carbide Corporation, Carbon Products Division, New York, NY.
[30] Birgeneau R J, Heiney P A and Pelz J P 1982 *Physica* B **109** & **110** 1785
[31] Ecke R E and Dash J G 1983 *Phys. Rev.* B **28** 3738
[32] Reynolds W N 1968 *Physical Properties of Graphite* (Amsterdam: Elsevier)
[33] Amelinckx S, Delavignette P and Heerschap M 1965 *Chemistry and Physics of Carbon* vol 1, ed P L Walker Jr (New York: Marcel Dekker) p 1
[34] Amelinckx S and Delavignette P 1960 *J. Appl. Phys.* **31** 2126
[35] Palache C 1941 *Am. Mineral.* **26** 709
[36] Freise E J and Kelly A 1962 *Proc. R. Soc.* A **264** 269
[37] Baker C, Gillin L M and Kelly A 1966 *Proc. 2nd Industrial Carbon and Graphite Conf.* (London: Society of Chemical Industry) p 132
[38] Calisti S, Suzanne J and Venables J A 1982 *Surf. Sci.* **115** 455
[39] Demétrio de Souza J L M, Rapp R E, de Souza E P and Lerner E 1984 *J. Low Temp. Phys.* **55** 273
[40] Krim J and Dash J G 1985 *Surf. Sci.* **162** 421
[41] Zhu Da-Ming 1988 *PhD Thesis* University of Washington
[42] Pengra D B 1991 *PhD Thesis* University of Washington
[43] Dietrich S and Schick M 1986 *Phys. Rev.* B **33** 4952

[44] Stewart G A and Dash J G 1970 *Phys. Rev.* A **2** 918
[45] Ihm G, Cole M W, Toigo F and Scoles G 1987 *J. Chem. Phys.* **87** 3995
[46] Dash J G and Puff R D 1981 *Phys. Rev.* B **24** 295
[47] Fisher M E and Berker A N 1982 *Phys. Rev.* B **26** 2507
[48] Imry Y 1980 *Phys. Rev.* B **21** 2042
[49] Challa M S S, Landau D P and Binder K 1986 *Phys. Rev.* B **34** 1841
[50] Bohr J 1992 private communication
[51] Ecke R E, Dash J G and Puff R D 1981 *Phys. Rev.* B **26** 1288
[52] Pengra D B 1991 unpublished